A Theoretical Study of the Molecular Mechanism for the Oxidation of Methanol by PQQ

J. Andrés,* V. Moliner, L. R. Domingo,† M. T. Picher,† and J. Krechl‡

Contribution from the Department of Experimental Sciences, Universitat Jaume I, Apartat 242, 12080 Castelló, Spain

Received November 18, 1994®

Abstract: As a model of chemical reactions that take place in the active site of methanol dehydrogenase, the molecular mechanism for the oxidation of methanol by the coenzyme PQQ (pyrroloquinolinequinone) has been characterized by different theoretical methods: AM1 and PM3 semiempirical procedures, ab initio method at 3-21G, 6-31G, and 6-31G** basis set levels, second order Møller–Plesset perturbation method and calculations based on density functional theory. We examine three possible molecular mechanisms. The first two reaction pathways are based on the nucleophilic attack of methanol oxygen on both quinone groups of PQQ. An analysis of a modified version of More O'Ferrall–Jencks diagrams shows that the overall process is a stepwise mechanism. The first step corresponds to the formation of a hemiketal intermediate, the transition structure (TS1) being a four-membered ring. The second step is associated with the decomposition of this intermediate and with the formation of formaldehyde. The TS2 can be described as a six-membered ring. The third molecular mechanism is associated with the hydride and proton transfers between the methanol and both carbonylic oxygens of PQQ. The corresponding transition structure (TS3) is a eight-membered ring and an analysis of a modified version of More O'Ferrall–Jencks diagrams and the transition vector for TS3 reveals an asynchronous pathway, describing this molecular mechanism as an initial hydride transfer followed by the proton transfer. The barrier heights for the three alternative reaction pathways are similar, showing that they are competitive molecular mechanisms. The geometries of the stationary structures and the transition vector associated with TSs on potential energy surfaces show many similarities and the dependence of these properties upon model systems and theoretical methods are analyzed and discussed.

1. Introduction

Methanol dehydrogenase is a bacterial quinoprotein which catalyzes the oxidation of methanol to formaldehyde in different methylotrophic and autotrophic bacteria.[1] Salisbury et al.[2] have isolated its redox cofactor from methylotrophic bacteria and based on its name, 2,7,9-tricarboxy-1*H*-pyrrolo[2,3-*f*]-quinoline-4,5-dione, the semisystematic name pyrroloquinolinequinone (PQQ), **1** (Figure 1a), has been accepted. While originally quinoproteins seemed restricted to some specialized microbes, nowadays it appears in a wide variety of organisms ranging from bacteria to mammals.[3,4] Since the large part of these enzymes are involved in the degradation or biosynthesis of bioregulators, it is already clear that an impact can be expected in the field of pharmacology and nutrition.[5] The potential importance of these bacteria to biotechnology and the characterization of its coenzyme has stimulated different research activities on the biochemical roles of PQQ-mediated redox cycling in biological processes.[6] Despite the active interest, the main reason for the lack of progress in understanding this dehydrogenase is due to ignorance of the nature of the reaction mechanism for methanol dehydrogenase and the role of the enzyme-bound PQQ in catalysis.[7]

Computational chemistry has already secured its position as an indispensable tool for rationalizing and understanding many features of enzyme catalysis. Different authors have amply documented the main problems associated with the application of quantum mechanics to analyzing the enzymatic reactions and the current state of this field.[8–12] To assist biological works, a theoretical study on molecular mechanisms for the oxidation of methanol to formaldehyde by model systems of PQQ has been carried out. The potential energy surface has been explored and the stationary points: reactants, products, intermediates, and transition structure (TS) have been characterized by different theoretical methods.

Semiempirical methods can be used for somewhat larger systems, but in this case only comparison with experiments or more sophisticated calculations can be used to judge the quality of the results. The simplest conventional ab initio methods may be used to determine geometries with the least computation cost, but in many cases the accuracy of the Hartree–Fock (HF) methods is not sufficient. In these cases it is necessary to perform the structure optimization which takes into account electron correlation effects in order to obtain a more satisfactory agreement.[13] Nevertheless, the corresponding calculations, perturbation theory, configuration interactions, or coupled-cluster

† Permanent address: Departament de Química Orgánica, Universitat de Valencia, 46100 Burjassot, Valencia, Spain.

‡ Permanent address: Department of Organic Chemistry, Institute of Chemical Technology, 166 28 Prague 6, Czech Republic.

® Abstract published in *Advance ACS Abstracts,* August 1, 1995.

(1) Anthony, C. *Principles and Applications of Quinoproteins*; Marcel Dekker: New York, 1993; pp 17–45.

(2) Salisbury, S. A.; Forrest, H. S.; Cruse, W. B. T.; Kennard, O. *Nature* **1979**, *280*, 843.

(3) Duine, J. A.; Frank, J.; Verwiel, P. E. J. *Eur. J. Biochem.* **1980**, *108*, 187.

(4) Duine, J. A.; Frank, J.; Jongejan, J. A. *FEMS Microbiol. Rev.* **1986**, *32*, 165.

(5) Rucker, R.; Killgore, J.; Duich, L.; Romero-Chapman, N.; Smidt, C.; Tinker, D. *Nutritional Essentiality of Pyrroloquinoline Quinone*; Kluwer Academic Publishers: The Netherlands, 1989.

(6) Xu, F.; Mack, C. P.; Quindt, K. S.; Shlafer, M.; Massey, V.; Hultquist, D. E. *Biochem. Biophys. Res. Comm.* **1993**, *193*, 434.

(7) Harris, T. K.; Davidson, V. L. *Biochemistry* **1993**, *32*, 4362.

(8) Warshel, A. *Computer Modeling of Chemical Reactions in Enzymes and Solutions*; New York, 1991.

(9) Warshel, A. *Curr. Op. Struct. Biol.* **1992**, *2*, 230.

(10) Merz, K. M. J. *Curr. Op. Struct. Biol.* **1993**, *3*, 234.

(11) Kollman, P. A. *Curr. Op. Struct. Biol.* **1992**, *2*, 765.

(12) Williams, I. H. *Chem. Soc. Rev.* **1993**, 277.

0002-7863/95/1517-8807$09.00/0

techniques impose serious limitations on the size of the system due to their computational cost. Recently, much interest has been given to methods based on density functional theory (DFT)[14] as an alternative to ab initio schemes in the kind of studies mentioned above[15,16] owing to its reduced computational requirements. Furthermore, since it takes into account most of the dynamical and nondynamical correlation effects, DFT is being successfully used in predicting various molecular properties with results of a quality comparable to the conventional post HF.[17-23]

This work can be considered as part of a project to study TS for different molecular mechanisms in the active site of enzymes.[24-35] In the present paper, a theoretical study was carried out for the oxidation reaction of methanol by PQQ as an example of the biochemical process in the active site of methanol dehydrogenase.

In section 2, we briefly outline the methods of calculation used for the present study. In section 3, we have described and discussed the results. The analysis of the structure of stationary points on the potential energy surface and the transition vectors allows us to decide which variables control the transformation. Changes of bond orders along the reaction pathway explain the nature of the process. A short conclusions section closes this paper.

2. Method and Model

Semiempirical calculations, AM1[36] and PM3,[37] were carried out using the MOPAC93[38] and the ab initio calculations have been performed with the GAUSSIAN 92/DFT series of programs[39] at HF/3-21G, HF/6-31G, and HF/6-31G** basis set levels. Electron correlation effects were considered via the second order Møller–Plesset perturbation (MP2) method.[40,41] We also employed methods based on density functional theory (DFT),[42,43] which has recently received increasing attention.[44] Thus, we employed the Becke's exchange functional,[45,46] which includes the Slater exchange along with corrections involving the gradient of the density and the gradient corrections provided by the Perdew 86 expression, along with his 1988 local correlation functional (BP).[47-49] These calculations have been carried out in conjunction with the 6-31G* basis set and high accuracy grid and integrals were used in all DFT calculations.

The exact characterization of the TS structures was achieved by using a simple algorithm,[34,35,50] in which the set of coordinates describing the system is separated into two: (qi) and (qj), where (qi) is the control space set which is responsible for the unique negative eigenvalue in the respective force constant matrix connected with variables that form the transition vector.[51] The remaining coordinates, set (qj), is called complementary space. First, the potential energy surface was explored in the quadratic region of the TS. The transition vector was determined by diagonalizing the force constant matrix. As a second step we optimized the complementary space using the OC method.[52] In the third step, a complete analytical optimization was achieved for the complete space of all variables. The optimizations were terminated after the threshold value of maximum displacement was 0.0018 Å and that of maximum force was 0.00045 hartree/bohr using the Berny analytical gradient optimization routine[53,54] in the GAUSSIAN 92/DFT program. Finally, the nature of each stationary point was established by calculating analytically and diagonalizing the matrix of energy second derivatives to determine the number of imaginary frequencies, zero for a local minimum and one for a transition state.

The first model of PQQ, comprising 36 atoms, was established according to X-ray findings[55] and our previous results[56,57] and (due to its size) is accessible only by semiempirical methods and corresponds to the complete molecular system, a bis-(quinone) tricarboxylic acid **1** (methoxatin, Figure 1a). The second model is reduced to a simple molecular system, *o*-benzoquinone **2** in the α-diketo form (Figure 1b). A comparison between the results obtained for both models is

(13) Hehre, W. J.; Radom, L.; Schleyer, P. v. R.; Pople, J. A. *Ab initio Molecular Orbital Theory*; John Wiley & Sons: New York, 1986.
(14) Labonowsky, J. K.; Andzelm, J. *Density Functional Methods in Chemistry*; Springer-Verlag: New York, 1991.
(15) Fan, L.; Ziegler, T. *J. Chem. Phys.* **1990**, *92*, 3645.
(16) Fan, L.; Ziegler, T. *J. Am. Chem. Soc.* **1992**, *114*, 10890.
(17) Sosa, C.; Andzelm, J.; Elkin, B. C.; Wimmer, E.; Dobbs, K. D.; Dixon, D. A. *J. Phys. Chem.* **1992**, *96*, 6630.
(18) Berces, A.; Ziegler, T. *J. Chem. Phys.* **1993**, *98*, 4793.
(19) Handy, N. C.; Murray, C. W.; Amos, R. D. *J. Phys. Chem.* **1993**, *97*, 4392.
(20) Seminario, J. M. *Chem. Phys. Lett.* **1993**, *206*, 547.
(21) Johnson, B. G.; Gill, P. M. W.; Pople, J. A. *J. Chem. Phys.* **1993**, *98*, 5612.
(22) Estrin, D. A.; Paglieri, L.; Corongiu, G. *J. Phys. Chem.* **1994**, *98*, 5653.
(23) Carpenter, J. E.; Sosa, C. P. *J. Mol. Struct. (Theochem)* **1994**, *311*, 325.
(24) Tapia, O.; Cardenas, R.; Andres, J.; Colonna-Cesari, F. *J. Am. Chem. Soc.* **1988**, *110*, 4046.
(25) Tapia, O.; Andres, J.; Aullo, J. M.; Cardenas, R. *Theochem.* **1988**, *166*, 421.
(26) Tapia, O.; Cardenas, R.; Andres, J.; Krechl, J.; Campillo, M.; Colonna-Cesari, F. *Int. J. Quantum. Chem.* **1991**, *39*, 767.
(27) Tapia, O.; Andrés, J.; Safont, V. S. *J. Phys. Chem.* **1994**, *98*, 4821.
(28) Andrés, J.; Safont, V. S.; Tapia, O. *Chem. Phys. Lett.* **1992**, *198*, 515.
(29) Andrés, J.; Safont, V. S.; Queralt, J.; Tapia, O. *J. Phys. Chem.* **1993**, *97*, 7888.
(30) Andrés, J.; Moliner, V.; Krechl, J.; Silla, E. *J. Chem. Soc., Perkin Trans. 2* **1993**, 521.
(31) Andrés, J.; Moliner, V.; Krechl, J.; Silla, E. *Bioorg. Chem.* **1993**, *21*, 260.
(32) Andrés, J.; Moliner, V.; Krechl, J.; Silla, E. *Int. J. Quantum Chem.* **1993**, *45*, 433.
(33) Andrés, J.; Moliner, V.; Krechl, J.; Silla, E. *J. Phys. Chem.* **1994**, *98*, 3664.
(34) Andrés, J.; Moliner, V.; Safont, V. S. *J. Chem. Soc., Faraday Trans.* **1994**, *90*, 1703.
(35) Tapia, O.; Andrés, J.; Safont, V. S. *J. Chem. Soc., Faraday Trans.* **1994**, *90*, 2365.
(36) Dewar, M. J. S.; Zoebisch, E. G.; Healy, E. F.; Stewart, J. J. P. *J. Am. Chem. Soc.* **1985**, *107*, 3902.
(37) Stewart, J. P. *J. Comput. Chem.* **1989**, *10*, 209.
(38) Stewart, J. J. P. In Fujitsu Ltd.: Tokyo, 1993.
(39) Frisch, M. J.; Trucks, G. W.; Head-Gordon, M.; Gill, P. M. W.; Wong, M. W.; Foresman, J. B.; Johnson, B. G.; Schlegel, H. B.; Robb, M. A.; Replogle, E. S.; Gomperts, R.; Andrés, J. L.; Raghavachari, K.; Binkley, J. S.; Gonzalez, C.; Martin, R. L.; Fox, D. J.; Defrees, D. J.; Baker, J.; Stewart, J. J. P.; Pople, J. A. GAUSSIAN92/DFT; Gaussian Inc.: Pittsburgh, PA, 1993.
(40) Binkley, J. S.; Pople, J. *Int. J. Quantum Chem.* **1975**, *9*, 229.
(41) Pople, J. A.; Binkley, J. S.; Seeger, R. *Int. J. Quant. Chem. Symp.* **1976**, *10*, 1.
(42) Andzelm, J.; Wimmer, E. *J. Chem. Phys.* **1992**, *96*, 1280.
(43) Sim, F.; St-Amant, A.; Papai, I.; Salahub, D. R. *J. Am. Chem. Soc.* **1991**, *114*, 4391.
(44) Gill, P. M. W.; Johnson, B. G.; Pople, J. A.; Frisch, M. *J. Chem. Phys. Lett.* **1992**, *197*, 499.
(45) Becke, A. D. *Phys. Rev. A* **1988**, *38*, 3098.
(46) Becke, A. D. *J. Chem. Phys.* **1993**, *98*, 5648.
(47) Perdew, J. P.; Yue, W. *Phys. Rev. B* **1986**, *33*, 8800.
(48) Perdew, J. P. *Electronic Structure of Solids*; Akademie Verlag: Berlin, 1991.
(49) Perdew, J. P.; Wang, Y. *Phys. Rev. B* **1992**, *45*, 13244.
(50) Tapia, O.; Andres, J. *Chem. Phys. Lett.* **1984**, *109*, 471.
(51) McIver, J. W. *Acc. Chem. Res.* **1974**, *7*, 72.
(52) Schlegel, H. B. Thesis, Queen's University, Kingston, Canada, 1975.
(53) Schlegel, H. B. *J. Comp. Chem.* **1982**, *3*, 214.
(54) Schlegel, H. B. *J. Chem. Phys.* **1982**, *77*, 3676.
(55) Koningsveld, V.; Jansen, H.; Jongejan, J. C.; Frank, J.; Duine, J. A. *Acta Crystallogr.* **1985**, *41*, 89.
(56) Krechl, J.; Bohm, S.; Kutham, J. *Collect. Czech. Chem. Commun.* **1989**, *54*, 1203.
(57) Andres, J.; Moliner, V.; Krechl, J. *Bioorg. Chem.* **1994**, *22*, 58.

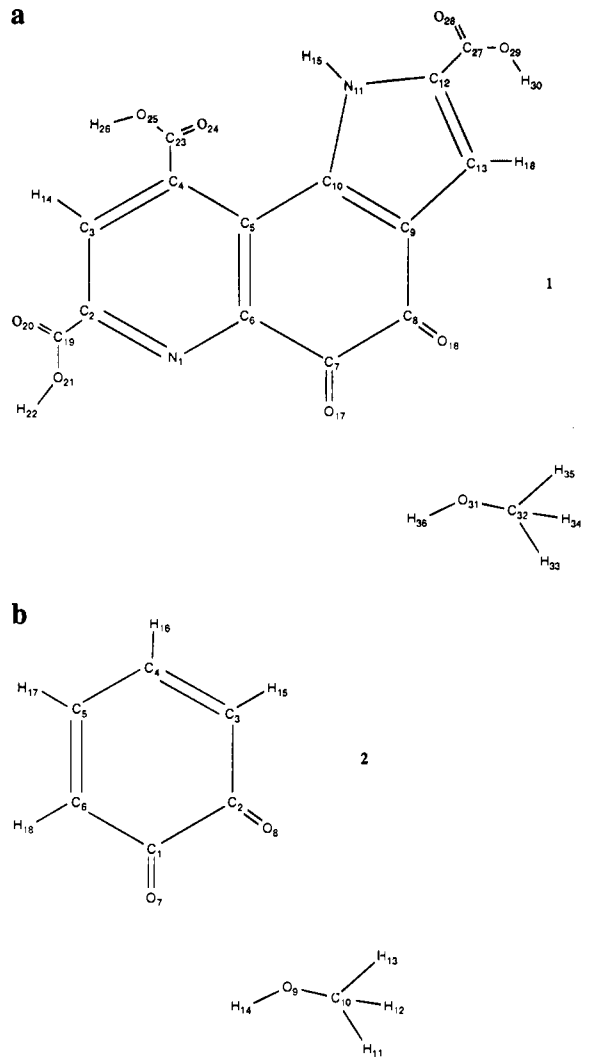

Figure 1. (a) Model **1**, structure of the PQQ prosthetic group of methanol dehydrogenase and (b) model **2**. Numbering of the atoms is included.

carried out; the geometical invariance of the fragments and the capability of the different theoretical approaches may be tested.

Analytical harmonic frequencies were computed for all stationary structures. Minima and TS have been characterized by the number of negative eigenvalues of the corresponding Hessian matrices (minima with 0, TS with 1 imaginary frequency).

This work has required a large amount of CPU time and calculations were performed on a cluster of Hewlett-Packard 9000/730 workstations at the Centre de Procés de Dades de la Universitat Jaume I de Castelló and on a IBM RS6000 workstation.

3. Results and Discussion

3.1. Structures of Stationary Points. According to our previous PM3 semiempirical study,[57] the overall process is a stepwise mechanism where the first step corresponds to the nucleophilic attack of methanol oxygen on the carbonyl group which is adjacent to the pyridine ring (C7 on model **1**). The hemiketal is decomposed in a second step forming the formaldehyde and the reduced PQQ (PQQH2). From that study the possible protonation of the nitrogen in the pyridine ring can be discarded.[57] In the present work we have studied, by PM3 and AM1 semiempirical procedures, the nucleophilic attack of methanol oxygen on both carbonyl groups (C7 and C8 on model **1**) of PQQ. These processes are depicted in Figure 2a as **I** → **IIa** → **III** and **I** → **IIb** → **III**.

For model **1**, the geometrical parameters for all stationary structures, presented in Tables 1 and 2, obtained with both semiempirical methods, reveal slight differences. The results show that the molecular mechanism can be interpreted as stepwise. Reactants, **I**, undergo protonation of O17 or O18 and nucleophilic attack on C7 or C8 roughly proportionally until the transition state, TS1, is achieved. **II** intermediate undergoes internal protonation of O17 or O18 by hydrogen H35 until the transition state, TS2, is achieved. In this second step, while hydrogen H35 is approaching the oxygen O18, the distance between O31 and C7, or O31 and C8, is not changing appreciably from the **II** distance of a single bond. Once the TS2 is achieved, the oxygen atom O31 with the rest of the forming formaldehyde is thus "jumping" off the formed PQQH2, and the distance where it is stabilized refers to complete separation of both components of the supermolecule **III**.

The analysis of the geometrical parameters for the **I** → **II** step reveals that the reaction occurs through a four-centered TS1 in which the reaction control depends on the position of the O31, H36, O17, and C7 atoms for the **I** → **IIa** process, and O31, H35, O18, and C8 for the **I** → **IIb** process. The TSs for processes **IIa** → **III** and **IIb** → **III** (TS2a and TS2b, respectively) depend on the position of six atoms: C7, C8, O18, O31, H33, and C32 for process **IIa** → **III** and C7, C8, O17, O31, H33, and C32 for process **IIb** → **III**.

The transition vector yields very concisely the essentials of the chemical process under study.[51] The perusal of amplitudes in the transition vector for TS1 and TS2 is associated with the atomic positions mentioned above. The normal mode analysis of TS1a, TS1b, TS2a, and TS2b yields a relatively high imaginary frequency, oscillating between 1020 and 2128 cm^{-1}. For TS1a, the negative force constant associated with H36–O17 is responsible for the imaginary frequency in both semiempirical methods, this variable being the major component of the transition vector. For TS2a, the negative eigenvalue arises from the cross terms in the force constant matrix; diagonal force constants are all positive. The major components of the transition vector are associated with O21–C7 and O18–H33 bond distances. Comparable results are obtained for process **I** → **IIb** → **III**. For TS1b, the negative force constant associated with H36–O18 is responsible for the imaginary frequency for both semiempirical methods, this variable being the major component of the transition vector. For TS2b, the negative eigenvalue arises also from the cross terms in the force constant matrix. The major components of the transition vector are associated with O31–C8 and O17–H33 bond distances.

In Table 3 the bond distances obtained with the different theoretical procedures of the stationary structures for model **2** are listed, and Figure 3 shows the geometry of TS1 and TS2. The interatomic distances of the stationary structures obtained with the three basis sets levels, the MP2 method, and the results that were obtained based on the DFT are quite similar and present significant invariance compared with the semiempirical results and compared with the results obtained with model **1**. However, the DFT results produce an overestimation of both distances including hydrogen atoms by about 0.01–0.03 Å (see Table 3). This geometrical agreement and the overestimation result have been noticed by other workers using local and nonlocal correction functionals.[21-23]

The normal mode analysis of TS1 and TS2 yields a relatively high imaginary frequency, oscillating between 1500i and 2100i and between 1200i and 2200i cm^{-1}, respectively. For TS1, the negative force constant associated with O17–H14 is responsible

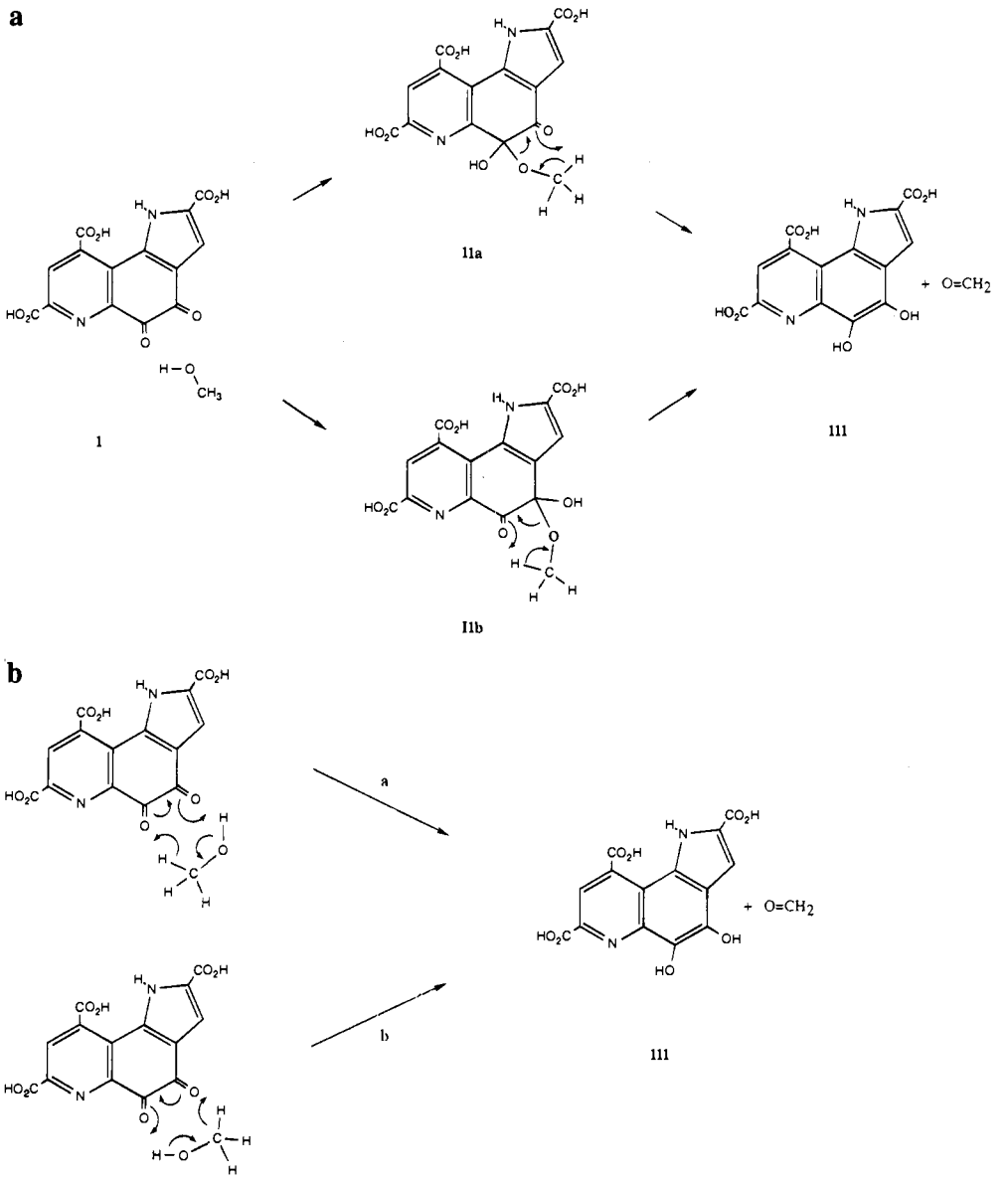

Figure 2. (a) Schematic representation of stationary points (R, intermediates, and P) for the oxidation reaction of methanol of PQQ. (a) Stepwise mechanism: nucleophilic attack of methanol oxygen O31 on carbon C7 (**I** → **IIa** → **III**) and C8 (**I** → **IIb** → **III**). (b) Concerted mechanism: hydride transfer from C32 to O17 (profile "a") and O18 (profile "b"). The proton transfer takes place between O31 and O18 or O17, respectively.

Table 1. Bond Distances (in Å) for the Stationary Points Obtained with the Different AM1 and PM3 methods[a]

	H36-O17		O31-C7		H36-O31		O17-C7	
	AM1	PM3	AM1	PM3	AM1	PM3	AM1	PM3
I	2.254	2.641	2.917	3.747	0.967	0.950	1.228	1.209
TS1	1.435	1.390	1.534	1.504	1.230	1.188	1.338	1.341
II	0.971	0.957	1.419	1.414	2.135	1.856	1.409	1.401
	H35-O18		H35-C32		O31-C7		O31-C32	
	AM1	PM3	AM1	PM3	AM1	PM3	AM1	PM3
II	2.652	2.681	1.118	1.096	1.419	1.414	1.419	1.404
TS2	1.118	1.059	1.530	1.569	1.607	1.612	1.318	1.313
III	0.978	0.962	3.110	2.661	4.343	3.913	1.229	1.206

[a] Nucleophilic attack of methanol oxygen O31 on carbon C7 using model **1**.

Table 2. Bond Distances (in Å) for the Stationary Points Obtained with the Different AM1 and PM3 method[a]

	H36-O18		O31-C8		H36-O31		O18-C8	
	AM1	PM3	AM1	PM3	AM1	PM3	AM1	PM3
I	2.254	2.641	2.917	3.747	0.967	0.950	1.228	1.209
TS1	1.429	1.377	1.561	1.535	1.229	1.192	1.333	1.334
II	0.969	0.950	1.422	1.419	2.456	2.325	1.409	1.397
	H35-O17		H35-C32		O31-C8		O31-C32	
	AM1	PM3	AM1	PM3	AM1	PM3	AM1	PM3
II	4.630	3.908	1.117	1.096	1.422	1.419	1.420	1.401
TS2	1.128	1.061	1.511	1.554	1.595	1.591	1.321	1.316
III	0.978	0.962	3.110	2.661	4.343	3.913	1.229	1.206

[a] Nucleophilic attack of methanol oxygen O31 on carbon C8 using model **1**.

for the imaginary frequency in all cases, this variable being the major component of the transition vector. For TS2, the negative force constant associated with C10−H13 is responsible for the imaginary frequency, except in the PM3 and 3-21G calculations where the negative eigenvalue arises from the cross terms in the force constant matrix; diagonal force constants are all positive. The major components of the transition vector are associated with O9−C1 and C10−H14 bond distances. These results are similar to those obtained with model **1**.

In order to complete this study, we have carried out an intensive search to find a third reaction pathway corresponding to a concerted mechanism associated with a hydride transfer,

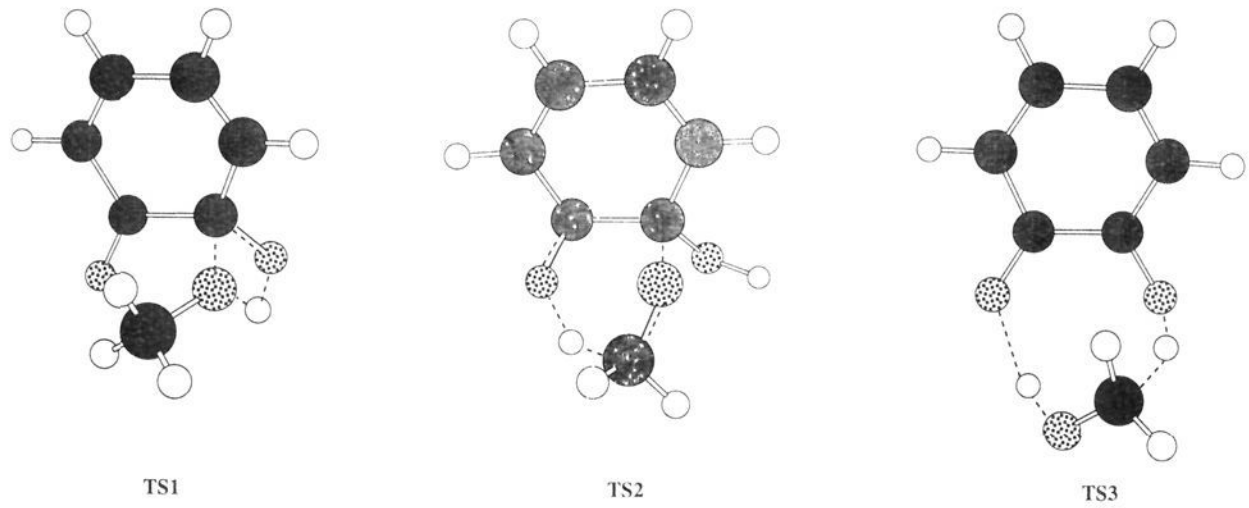

Figure 3. A schematic representation of the TS1, TS2, and TS3 geometries for model **2**.

Table 3. Bond Distances (in Å) for the Stationary Points Obtained by Semiempirical AM1 and PM3 Calculations and by ab Initio HF/3-21G, HF/6-31G, HF/6-31G**, and RBP86/6-31G* Calculations[a]

	H14-O7						O9-C1					
	3-21G	6-31G	6-31G**	BP	AM1	PM3	3-21G	6-31G	6-31G**	BP	AM1	PM3
I												
TS1	1.340	1.347	1.340	1.352	1.430	1.382	1.683	1.637	1.683	1.683	1.556	1.526
II	0.970	0.956	0.948	0.993	0.970	0.971	1.428	1.424	1.395	1.456	1.428	1.423
	H14-O9						O7-C1					
	3-21G	6-31G	6-31G**	BP	AM1	PM3	3-21G	6-31G	6-31G**	BP	AM1	PM3
I	0.963	0.949	0.940	0.975	0.963	0.947	1.211	1.215	1.188	1.231	1.233	1.214
TS1	1.157	1.159	1.157	1.178	1.224	1.188	1.328	1.344	1.329	1.320	1.339	1.340
II	2.456	2.412	2.415	2.581	2.259	2.322	1.406	1.400	1.374	1.392	1.409	1.398
	H13-O8						H13-C10					
	3-21G	6-31G	6-31G**	BP	AM1	PM3	3-21G	6-31G	6-31G**	BP	AM1	PM3
II	3.009	2.956	2.904	2.749	3.189	3.218	1.078	1.081	1.086	1.109	1.119	1.093
TS2	1.136	1.208	1.278	1.302	1.148	1.076	1.472	1.398	1.472	1.472	1.477	1.532
III	0.967	0.953	0.942	0.978	0.970	0.948						
	O9-C1						O9-C10					
	3-21G	6-31G	6-31G**	BP	AM1	PM3	3-21G	6-31G	6-31G**	BP	AM1	PM3
II	1.428	1.424	1.395	1.457	1.428	1.423	1.442	1.435	1.403	1.431	1.416	1.402
TS2	1.679	1.787	1.679	1.679	1.605	1.573	1.366	1.318	1.358	1.361	1.323	1.324
III							1.207	1.210	1.185	1.216	1.227	1.202

[a] Nucleophilic attack of methanol oxygen O9 on carbon C1 using model **2**.

H35, between C32 and O18 or O17, and a proton transfer, H36, between O31 and O17 or O18, respectively (model **1**). These alternative pathways are depicted in Figure 2b. We have characterized the transition structures (TS3a and TS3b) where the reaction coordinate vibrational mode comprises motion of the hydride and proton transfers. From a geometrical point of view TS3a and TS3b are quite similar, and the hydride transfer is more advanced than the proton transfer. These findings show that both transfers are dynamically uncoupled but kinetically coupled and the negative eigenvalue for these TSs is associated with the geometrical variables mentioned above.

Similar calculations has been carried out with model **2** (hydride transfer, H13, between C10 and O8, and a proton transfer, H14, from O9 to O7). The results obtained with this model, listed in Table 4 as TS3, are similar to those obtained with model **1** and seem to be qualitatively independent on the computational method. Nevertheless, it is important to point out the large value of the interatomic distance H14−O7 obtained with AM1 compared with the rest of the methods. TS3 for model **2** is depicted in Figure 3. The normal mode analysis of TS3 renders a high imaginary frequency for the Hartree−Fock method (2454i−2560i cm^{-1}), for the AM1 semiempirical procedure it is 1133.5 cm^{-1}, for the BP it is 1064.5i cm^{-1}, while the PM3 semiempirical method presents a low value of 623.3i cm^{-1}. For all methods, the negative eigenvalue arises from the cross terms in the force constant matrix; diagonal force constants are all positive and the major components of the transition vactor are associated with H13−O8 and C10−H13 bonds (hydride transfer), H14−O7 and H14−O9 bonds (proton transfer), and C10−H13−O8, H11−C10−H13, and H12−C10−H13 bond angles. These findings show a strong coupling of the H13 position in the bridge with both the intermolecular distance, C10−O8, and the orientation.

3.2. Energetics of Stationary Points. For model **1**, the energetic values for the structures **I**, TS1a, TS1b, **IIa**, **IIb**, TS2a, TS2b, TS3a, TS3b, and **III** are presented in Table 5. The barrier height is quite high, oscillating between 49.2 to 57.9 kcal/mol. Nevertheless, if we compare the two stepwise mechanisms, both semiempirical methods describe the **I** → **IIa** → **III** pathway energetically more favorably than the profile **I** → **IIb** → **III**. The activation energies of the two steps are slightly lower for the first pathway. The decomposition of the hemiketal would be the rate limiting step. It is important to remark on the accuracy of these results and the experimental data that prove how the quinone group adjacent to the pyridine ring is reactive toward nucleophilic agents.[58] On the other hand, the values of the activation energy for the concerted mechanism (49.6−57.9 kcal/mol) are quite similar to those obtained for the stepwise process, offering the possibility of a competitive mechanism. Furthermore, both semiempirical methods show the hydride

Table 4. Bond Distances (in Å) for the Transition States Obtained with the Different Methods Corresponding to the Concerted Mechanism[a]

	H35-O17		H35-C32		O17-C7		H36-O18	
	AM1	PM3	AM1	PM3	AM1	PM3	AM1	PM3
TS3a	1.086	1.020	1.550	1.602	1.323	1.316	2.001	1.736
	H35-O18		H35-C32		O18-C8		H36-O17	
	AM1	PM3	AM1	PM3	AM1	PM3	AM1	PM3
TS3b	1.068	0.999	1.605	1.696	1.330	1.334	1.982	1.704

	C1-O7						C2-O8					
	3-21G	6-31G	6-31G**	BP	AM1	PM3	3-21G	6-31G	6-31G**	BP	AM1	PM3
TS3	1.262	1.268	1.236	1.285	1.262	1.248	1.320	1.318	1.292	1.315	1.329	1.315
	H13-O8						C10-H13					
	3-21G	6-31G	6-31G**	BP	AM1	PM3	3-21G	6-31G	6-31G**	BP	AM1	PM3
TS3	1.183	1.137	1.119	1.196	1.078	1.025	1.412	1.454	1.451	1.361	1.565	1.585
	H14-O7						H14-O9					
	3-21G	6-31G	6-31G**	BP	AM1	PM3	3-21G	6-31G	6-31G**	BP	AM1	PM3
TS3	1.478	1.609	1.608	1.376	1.952	1.733	1.029	0.990	0.981	1.090	0.988	0.975

[a] TS3a and TS3b using model **1** and TS3 using Model **2**.

Table 5. Heat of Formation and Relative Energy to **I** (kcal/mol) in Parentheses Obtained by Semiempirical Calculations Using Model **1**

	AM1		PM3	
I	−278.8	(0.0)	−315.7	(0.0)
TS1a	−229.4	(49.4)	−266.4	(49.2)
TS1b	−226.1	(52.8)	−264.9	(50.7)
IIa	−284.2	(−5.4)	−317.1	(−1.5)
IIb	−283.5	(−4.7)	−313.2	(2.5)
TS2a	−229.2	(49.6)	−261.1	(54.6)
TS2b	−226.4	(52.4)	−259.7	(56.0)
III	−287.4	(−8.6)	−321.9	(6.2)
TS3a	−229.2	(49.6)	−264.1	(51.6)
TS3b	−223.3	(55.5)	−257.8	(57.9)

transfer to the quinone group adjacent to the pyridine ring to be more favorable (5.9 and 6.3 kcal/mol for AM1 and PM3, respectively) than the hydride transfer to alternative quinone group (C8=O18). The AM1 procedure describes an exothermic reaction, while the PM3 results shows an endothermic process.

In Table 6, the energy of stationary structures calculated with the different methods for model **2** is reported. In the stepwise mechanism, the passage from **I** to TS1 implies the formation of O9−C1 and H14−O7 bonds, the breaking of the H14−O9 bond and the C1=O7 double bond becomes single. On the other hand, the **II** to TS2 passage implies the formation of a O8−H13 bond, the breaking of the O9−C1 and C10−H13 bonds, the C2=O8 double bond becomes single, and the C1−C2 and O9−C10 single bonds become double, the interconversion from **II** to **III** being the rate limiting step for the stepwise mechanism.

The comparative analysis of the relative energies reveals quite high and comparable activation energies with respect to stepwise and concerted processes. Due to these transformations we could expect that taking the correlation energy into account would have an influence on the barrier height. The MP2 barrier energies are lower than those obtained within HF (at the three different basis set) and using semiempirical procedures. Calculations based on the DFT are even closer to the values that could be expected for a biological reaction (small activation energies). The DFT methods with local spin density approximations underestimate the barrier energies, while the inclusion of nonlocal corrections improves the compute barrier. This is in agreement with previous results of Johnson et al.[21] and Carpenter et al.[23]

Nevertheless, note that for approximate formulations, such as Hartree−Fock, Levy, and Perdew[59] showed that the change in the energy error, upon change in geometry, is zero through the second order perturbation term for Coulomb Hamiltonians. This may explain why approximate energy curves often closely parallel exact curves and give accurate geometries. Thus, this kind of calculation might be good enough for obtaining adequate geometries in a number of cases; absolute energies are usually unreliable.

3.3. Modified More O'Ferrall−Jencks Diagram. Bond orders variables are used by physical organic chemists to rationalize structure−reactivity correlation in reaction mechanisms,[60] and the relative change of the bond order can serve as a measure of the progress of chemical transformation.[61,62] In our study, Pauling bond orders,[63] n, were calculated through the expression: $n = \exp\{[R(1) - R(X)]/0.3\}$, where $R(X)$ is the length corresponding to bond order X and $R(1)$ is the reference bond length corresponding to bond order 1. For the bonds being broken the reference bond lengths for the single bonds were the equilibrium distances in the reactants. For the bonds being formed the reference values were the equilibrium distances in the products.

Particularly popular use has been made of a modified version of the More O'Ferrall−Jencks diagram.[64,65] This diagram is a two-dimensional map where the bond orders associated with bonds which are formed/broken in the chemical processes are depicted. The use of these diagrams for prediction of mechanism or TS changes has been well documented.[33,66] In semiempirical calculations for the nucleophilic attack of methanol on C7, model **1**, the diagram is composed of n(O17−C7)−n(O31−C7) vs n(O17−H36)−n(O31−H36) and n(O31−C7)−n(O31−C32) vs n(H35−C32)−n(H35−O18) for the first and second steps, respectively. For the nucleophilic attack of methanol on C8, model **1**, the diagram is composed of n(O18−C8)−n(O31−C8) vs n(O18−H36)−n(O31−H36) and n(O31−C8)−n(O31−C32) vs n(H35−C32)−n(H35−O17) for the first

(58) Dekker, R. H.; Duine, J. A.; Frank, J.; Verwiel, P. E. J.; Westerling, J. *Eur. J. Biochem.* **1982**, *125*, 69.
(59) Levy, M.; Perdew, J. P. *J. Chem. Phys.* **1986**, *84*, 4519.
(60) Formosinho, S. J. *J. Chem. Soc., Perkin Trans.* **1988**, 839.
(61) Lendvay, G. *J. Phys. Chem.* **1993**, *93*, 4422.
(62) Lendvay, G. *J. Phys. Chem.* **1994**, *98*, 6098.
(63) Pauling, L. *J. Am. Chem. Soc.* **1947**, *69*, 542.
(64) More O'Ferrall, R. A. *J. Chem. Soc. B* **1970**, 274.
(65) Jencks, W. P. *Acc. Chem. Res.* **1980**, *13*, 161.
(66) Barnes, J. A.; Wilkie, J.; Williams, I. H. *J. Chem. Soc., Faraday Trans.* **1994**, *90*, 1709.

Table 6. Energy of Stationary Structures Calculated with the Different Methods for Model 2[a]

	HF/3-21G		HF/6-31G		HF/6-31G**		MP2/6-31G*//HF/6-31G**		BP/6-31G*		AM1		PM3	
I	−491.484 794	(0.0)	−494.075 428	(0.0)	−494.273 066	(0.0)	−495.717 529	(0.0)	−497.152 313	(0.0)	−78.7493	(0.0)	−81.0157	(0.0)
TS1	−491.431 539	(33.4)	−493.968 027	(67.4)	−494.187 999	(53.4)	−495.671 033	(29.2)	−497.109 875	(26.6)	−31.8326	(46.9)	−35.1093	(45.9)
II	−491.510 579	(−16.2)	−494.053 500	(13.8)	−494.286 191	(−8.2)	−495.671 033	(−44.5)	−497.170 974	(−11.7)	−87.2173	(−8.5)	−86.4682	(−5.5)
TS2	−491.399 012	(53.8)	−493.939 740	(85.1)	−494.164 065	(68.4)	−495.667 984	(46.4)	−497.111 865	(25.4)	−34.5549	(44.2)	−32.5260	(48.5)
III	−491.525 465	(−25.5)	−494.079 323	(−2.4)	−494.303 328	(−19.0)	−495.758 889	(−57.0)	−497.181 885	(−18.6)	−97.9348	(−19.2)	−99.2301	(−18.2)
TS3	−491.395 286	(56.2)	−493.936 757	(87.0)	−494.155 326	(73.9)	−495.603 220	(71.7)	−497.155 910	(2.3)	−30.1393	(48.6)	−32.3839	(48.6)

[a] For semiempirical procedures, values of heat of formation are reported while values of total energy are listed for ab initio results. In parentheses relative energies to **I** in kcal/mol.

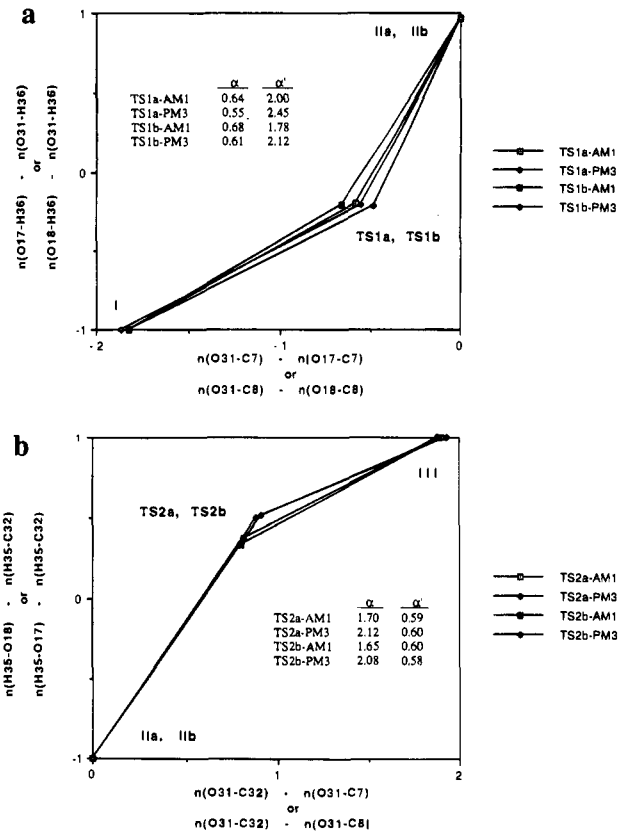

Figure 4. Modified More O'Ferrall–Jencks diagram obtained with semiempirical calculations for the stepwise mechanism, model **1**: (a) **I** to **II** step and (b) **II** to **III** step.

and second steps, respectively. The first step is depicted in Figure 4a, while the second step is presented in Figure 4b. The progress of the reaction pathways for the different steps are monitored by means of the corresponding slopes. Motion from reactants, **I** (bottom left corner of Figure 4a) to intermediate, **II** (top right corner Figure 4a) and motion from **II** (bottom left corner of Figure 4b) to products **III** (top right corner Figure 4b) are measured by α (**I-TS1**), α' (TS1-**II**) and β, (**II-TS2**), β' (TS2-**III**) slopes, respectively. A diagonal connecting reactants and products via TS would represent a synchronous process, while motions from reactants to the upper left or lower right corners would correspond to stepwise mechanisms. In these corners we would locate hypothetical stationary species with biradical or ionic characteristics or both.

The results depicted in these diagrams show a stepwise mechanism and both first and second steps like asynchronous reactions. The reaction pathways described by α and α' slopes are practically independent of the method. Nevertheless, the PM3 results describe the TSs in a more advanced stage of the reaction profile: smaller values of α and bigger values of α' for the first step and opposite results for the β and β' values. Values between 0.55 and 0.68 for α and between 1.78 and 2.45 for α' are calculated for the first step (Figure 4a), while the β and β' values are in a range of 1.65–2.12 and 0.58–0.60, respectively (Figure 4b).

For model **2**, similar results are depicted in Figures 5a and 5b. For the first step, **I** to **II**, the diagram is composed of n(O9–C1)–n(O7–C1) vs n(O7–H14)–n(O9–H14) (see Figure 5a). For the second step, **II** to **III**, we have used the following combination of bond orders: n(O9–C1)–n(O9–C10) vs n(H13–C10)–n(H13–O8) (see Figure 5b). Progress from reactants, **I** (bottom left corner of Figure 4a) to intermediate, **II** (top right corner Figure 5a) and **II** (bottom left corner of Figure 5b) to products **III** (top right corner Figure 5b) is measured by α (**I-**

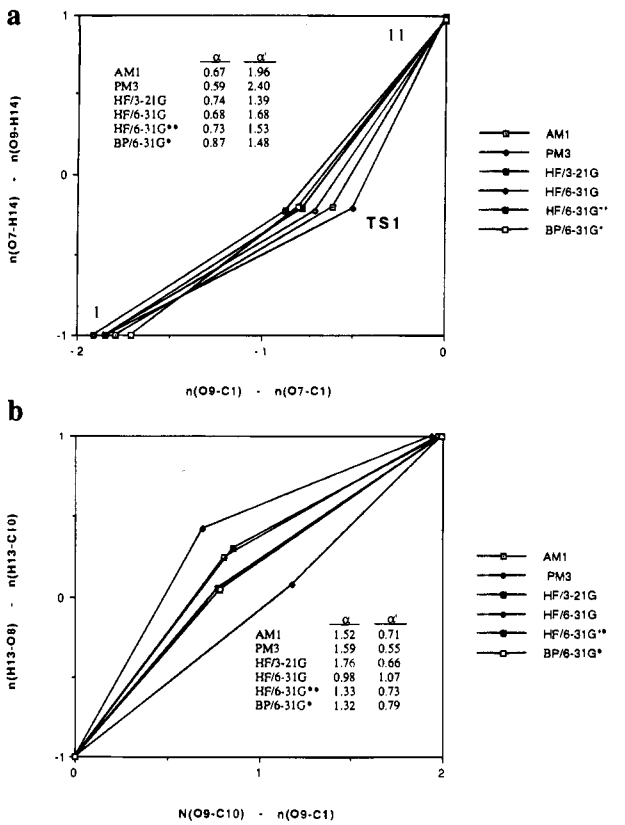

Figure 5. Modified More O'Ferrall–Jencks diagram obtained with the different calculations for the stepwise mechanism, model **2**: (a) **I** to **II** step and (b) **II** to **III** step.

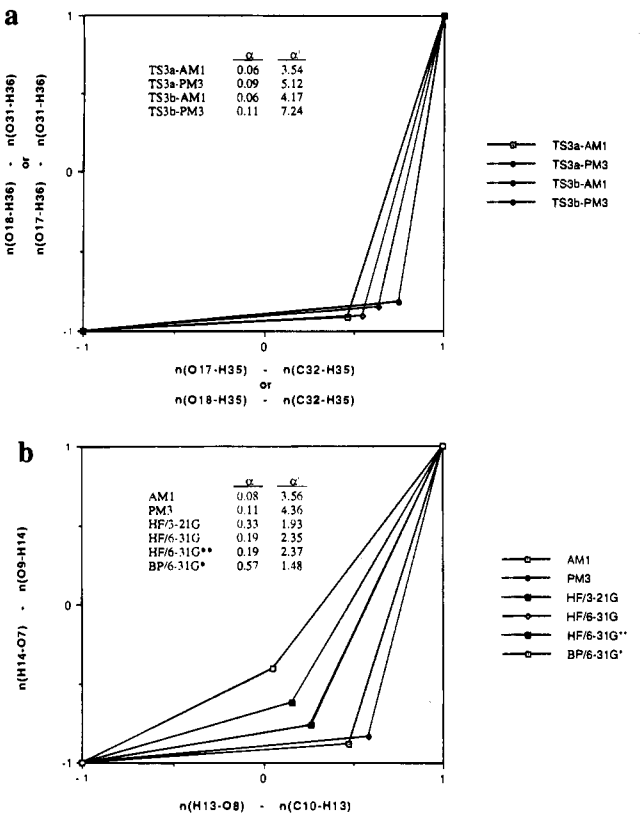

Figure 6. Modified More O'Ferrall–Jencks diagram obtained with the different calculations for the concerted mechanism: (a) model **1** and (b) model **2**.

TS1), α' (TS1-**II**) and β, (**II-TS2**), β' (TS2-**III**) slopes, respectively. Values between 0.59 and 0.87 for α and between 1.39 and 2.40 for α' are calculated for the first step, while the β and β' values are in a range of 0.98–1.76 and 0.55–1.07, respectively. It is important to point out two features: (i) the results obtained with model **1** are quite similar to those obtained with model **2**, and (ii) the reaction pathways described by the different slopes are practically independent of the method (the values describe the first and second steps like asynchronous reactions) except the HF/6-31G method which produces a nearly synchronous second step, and the PM3 method whose results describe the TSs in more advanced stages of the reaction profiles than with the **1** and **2** models.

Figure 6 shows similar diagrams for the third alternative pathway. In semiempirical calculations on model **1** (see Figure 6a), the diagram represents n(O17–H35)–n(C32–H35) vs n(O18–H36)–n(O31–H36) or n(O18–H35)–n(C32–H35) vs n(O17–H36)–n(O31–H36). For reactions studied with model **2**, we have used the following combination of bond orders: n(H13–O8)–n(C10–H13) vs n(H14–O7)–n(O9–H14) (see Figure 6b). In both maps, progress from reactants, **I** (bottom left corner), to TS3 (bottom right corner) and TS3 to products **III** (top right corner) is measured by α (**I-TS3**) and α' (TS3-**III**) slopes, respectively. The horizontal displacements correspond to the hydride tranfer, while the vertical motions represent the proton transfer. Values between 0.06 and 0.57 for α and between 1.48 and 7.24 for α' have been calculated. It is important to note the large differences between both slopes. This fact is in good agreement with the geometrical results: in the TS3 the hydride transfer is almost completed, while the proton transfer is still far away from the value obtained in products. Semiempirical methods, AM1 and PM3, render low values for α slopes (0.06–0.11) for model **1** and **2**, while the reaction pathway described by DFT calculations presents closer values for both slopes than semiempirical and Hartree–Fock methods.

4. Conclusions

This study represents a modelization of the molecular mechanism associated with the oxidation of methanol by the coenzyme PQQ (pyrroloquinolinequinone). The results presented in this paper are based on the geometry optimization done using AM1 and PM3 semiempirical methods and single configurational ab initio self-consistent field molecular-orbital theory at 3-21G, 6-31G, and 6-31G** basis set levels. We have also considered electron correlation effects at second order Møller–Plesset perturbation method and calculations based on DFT. The stationary points were located and characterized, and some important features were clarified. The results can be summarized as follows.

(I) The overall process may be a concerted or a stepwise mechanism, and only geometrical differences between the two possibilities have been found. A theoretical characterization of the TSs that control both alternative pathways is carried out.

(II) The stepwise mechanism presents a first step controlled by a simultaneous protonation of one of the quinone oxygen and the nucleophilic attack on its carbon thus forming the hemiketal intermediate. The second step, the decomposition of this hemiketal, is a reaction with a higher activation energy barrier.

(III) The concerted mechanism, associated with hydride and proton transfers between the methanol and both carbonylic oxygens of PQQ, reveals an asynchronous process. The TS3 is in an advanced stage for the hydride transfer and in an early stage for the proton transfer.

(IV) A comparative analysis of the stepwise and concerted mechanisms shows that the carbonyl carbon adjacent to the

pyridine ring is slightly more reactive in accordance with the experimental data.

(V) TS1 is described as a four-membered ring, TS2 depends on the position of six atoms, and TS3 is a eight-membered ring. Semiempirical and ab initio results reproduce the same qualitative features. Satisfactory agreement has been found for geometries of stationary points and frequencies of transition states.

(VI) The comparative analysis of the semiempirical and ab initio results obtained with two different molecular models prove the geometrical invariance of the fragments and the capability of the semiempirical approaches.

(VII) From an energetic point of view, MP2/6-31G*//HF/6-31G** and BP/6-31G* reproduce the smallest barrier energies. Nevertheless, the DFT methods have the advantage of being more efficient computationally than the MP2.

Acknowledgment. This work was supported by research funds of the Conselleria de Educació i Ciencia, Generalitat Valenciana (Project GV-1142/93) and DGICYT (Project PB93-0661). The authors are grateful to the Centre de Procés de Dades de la Universitat Jaume I for providing them with CPU time on the cluster of Hewlett Packard 9000/730 workstations. The final version of this paper has been substantially improved by the comments and criticisms raised by two referees. We would respectfully express our indebtedness to them.

Supporting Information Available: Tables S1−S4, listing Hessian unique negative eigenvalue, imaginary frequency (cm^{-1}), geometric parameters, force constants, and eigenvectors for the transition states on model **1** (TS1a, TS2a, TS1b, TS2b, TS3a, and TS3b) and model **2** (TS1, TS2, and TS3) (7 pages). This material is contained in many libraries on microfiche, immediately follows this article in the microfilm version of the journal, can be ordered from the ACS, and can be downloaded from the Internet; see any current masthead page for ordering information and Internet access instructions.

JA943889Q